Mater. Res. Soc. Symp. Proc. Vol. 1276 © 2010 Materials Research Society

Magnetic properties of bulk composite FeBSiM (M=Cr,Zr) alloys with high microhardness.

S. Báez[1], I. Betancourt[1], M. E. Hernandez-Rojas[2] and I. A. Figueroa[1].
[1]Departamento de Materiales Metálicos y Cerámicos, Instituto de Investigaciones en Materiales, Universidad Nacional Autónoma de México, México D.F. 04510, México.
[2]Departamento de Biotecnología, Departamento de Ingeniería de Procesos e Hidráulica, Universidad Autónoma Metropolitana-Iztapalapa, México D.F. 09340, México.

ABSTRACT

The synthesis, mechanical and magnetic properties of bulk composite $Fe_{72}B_{19.2}Si_{4.8}M_4$ (M=Cr, Zr) alloys obtained by a copper mould injection casting technique under a protective helium atmosphere are reported and discussed. The resultant microstructure of the composite alloys consists of crystalline $Fe_{92}Si_8$ and Fe_2B phases embedded in a glassy matrix. The values of microhardness (H_v) show maxima for the alloy containing Cr with 10.24±0.95 GPa. The maximum value of saturation magnetization average ($\mu_0 M_s$) is 1.25±0.02 T for Cr-containing alloy. The Curie temperatures (T_c) of amorphous phases are higher than 390 K for both alloys. However, the bulk composite alloys presents values for crystallization temperature (T_x) of 1289±10 K and 1140±10 K for Cr and Zr-containing alloys, respectively. These results are interpreted on the basis of the interplay between the crystalline and amorphous phases.

INTRODUCTION

Functional materials are a fundamental part of modern technology due to the increasing necessity of active and versatile solid components performing in a wide range of applications like sensing, actuating, gauging, controlling, monitoring, energy converting, replacing and storing [1, 2]. In particular, the widespread interest on magnetic materials has created an active research field that includes both fundamental investigation and technological applications, ranging from simple toys, to sophisticated imaging techniques devices for the human body [3, 4]. Most modern applications make use of conventional crystalline alloys, which have been studied in detail since the development of the first magnetic steels by the end of the XIX century [5, 6] and whose magnetic properties are determined to a large extent by the careful tailoring of (a) microstructure: phases, grain size and its distribution, grain boundaries, crystal defects, impurities and, (b) chemical composition, which influences intrinsic magnetic properties such as the $\mu_0 M_s$ (which corresponds to the atom magnetic moment per unit volume of the material; μ_0 is the magnetic permeability of free space), T_c (which indicates the temperature for the ferromagnetic-paramagnetic transition) and magnetocrystalline anisotropy (which refers to existence of easy axis for the magnetic polarization along specific unit cell directions). Less common amorphous alloys, characterized by a lack of atomic long range order, and thus, opposing to crystalline materials, have been subject of research interest since the announcement of the first metallic glass prepared by means of rapid solidification techniques [7]. For magnetic

amorphous alloys, the absence of crystallinity constitutes the main factor to produce materials with very high magnetic permeability and readily controllable magnetostriction (i.e. the ability of the alloy to modify its dimensions under the application of an external magnetic field, which strongly depends initially on the transition metals Fe, Co or Ni content). In both types of materials (crystalline and amorphous), the combination with good mechanical properties in general paves the way to more applicable materials with the ability, for instance, of sustaining a magnetic behavior under harsh working conditions such as continuous wear. The objective of the present study is to investigate the effects of small concentration of Cr and Zr on the synthesis, structural, mechanical (hardness) and magnetic properties of the injection cast FeBSiM (M=Cr, Zr) alloys.

EXPERIMENTAL TECHNIQUES

Fe-based alloy ingots of composition $Fe_{72}B_{19.2}Si_{4.8}M_4$ (M=Cr,Zr) are prepared by arc-melting with high purity (99.99 %) elements in a Ti-gettered inert Ar-atmosphere. The alloy compositions represent the nominal values but the processing weight losses are negligible (<0.1 %). The alloy ingots are inverted on the hearth and re-melted several times, in order to ensure compositional homogeneity. Cylindrical alloy rods having a single diameter of 3 mm and a length of ~55 mm are produced by copper mould injection casting under a protective He-atmosphere. The alloys microstructure is characterized by X-ray diffraction (XRD) with Cu-K_α radiation and a Ge primary monochromator (BRUCKER-AXS) is used to reduce the fluorescence of the XRD scan. Scanning Electron Microscopy (SEM) operated at 20 keV and 700 pA and Transmission Electron Microscopy (TEM) operated at 120 keV are also used to determine the structure of the as-cast alloys. The thermal stability of the amorphous phase within each bulk alloy is monitored by using Differential Thermal Analysis (DTA) at a heating rate of 20 K/min. The magnetic properties of the alloys are determined in a Vibrating Sample Magnetometer (VSM) with a maximum applied field of 500 kA/m and a Magnetic Thermogravimetric Analyzer (MTGA) with a heating rate of 10 K/min. The average values and the associated uncertainty are calculated after 10 measurements with fresh samples in every experiment. The H_v of the alloys is carried out using a commercial microhardness tester under a constant indentation load of 50 g during 20 s. The average values and the associated uncertainty are calculated after 20 indentations. The bulk composite alloys are placed in quartz tubes; the air is evacuated to a pressure of 3×10^{-5} kPa, then backfilled with 30 kPa argon and finally sealed. The samples are then heat treated at 1000 K for 8 hours. After this, the samples are removed from the furnace and left to cool down to room temperature.

RESULTS

The presence of the glassy structure and the crystalline phases is confirmed by XRD for both alloys, as shown in Figure 1. In this figure, the existence of diffraction peaks together with a broad maximum between $2\theta=40°$ and 55° can be seen. The resulting hump peak of the repeated XRD analysis appeared at ~43.56 for Cr and ~45.49 degrees for Zr. The differences between the

hump peaks could be attributed to changes in the composition. In the alloy with Cr (Fig. 1a) the well defined peaks located at 2θ=65.2° and 82.6°, coincide with the (200) and (211) planes of the $Fe_{92}Si_8$ phase. As for the Zr-containing alloy (Fig. 1b), the peaks located at 2θ=79.5° and 92.9°, coincide with the (330) and (332) planes of the Fe_2B phase.

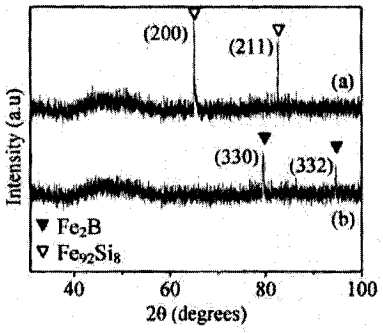

Figure 1. XRD patterns for both alloys: (a) $Fe_{72}B_{19.2}Si_{4.8}Cr_4$ and (b) $Fe_{72}B_{19.2}Si_{4.8}Zr_4$.

Figure 2. SEM backscattered electron images showing two distinguishable regions (I and II) for both alloys: (a) Cr-containing alloy and (b) Zr-containing alloy.

In addition, SEM backscattered electron images (Fig. 2) show two distinguishable regions (I and II) for the Cr and Zr-containing alloys. Zone I in both alloys (Figs. 2a-b) exhibits a defined structure of equiaxed grains, typical of crystalline phases [8]. Zone I in the Zr-containing alloy can be associated with the Fe_2B phase. In contrast for region II, no crystalline features are evident, and therefore this region is assumed to be the amorphous phase. This region has Fe, Si and Cr contents of ~74 at.%, 7.3 at.% and 2.7 at.%, respectively (according to EDS analysis). Bearing in mind that B cannot be detected in this technique, the measured compositions agree satisfactorily well with expectations for the bulk composite alloys. Similarly, for the Cr-containing alloy, region I can be associated to the $Fe_{92}Si_8$ crystalline phase, and region II to the amorphous phase. This region has an approximate Fe, Si and Zr content of ~75 at.%, 5.8 at.% and 2.9 at.% (EDS analysis).

In order to support the aforementioned results, a number of bulk samples are analyzed by TEM. The bright field (BF) images and SAD patterns taken from the cross section of the Zr alloy are shown in Figure 3. The pattern of Fig. 3a is taken from the marked zone in Figure 3b. It consists only of a diffuse halo with no distinctive evidence of crystalline rings (glassy zones). Figure 3c shows an indexed pattern taken from the encircled crystalline zone in Figure 3b. Here several rings corresponding to the crystalline phase Fe_2B are observed. These results are consistent with the XRD and SEM results shown earlier and therefore confirm that a composite structure is successfully produced for the Zr alloy rod.

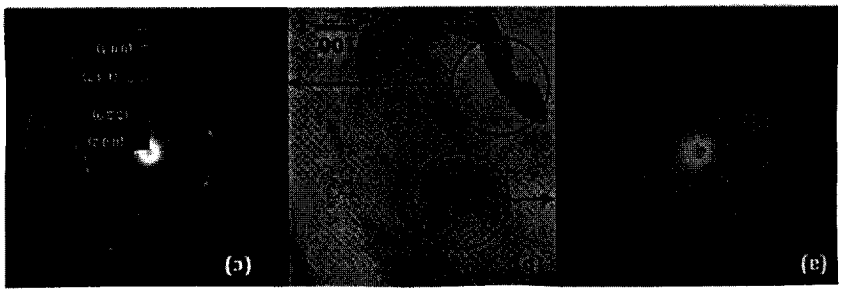

Figure 3. (a) TEM bright field image and (b) electron diffraction pattern taken from region I and (c) crystalline phase of the Zr containing alloy.

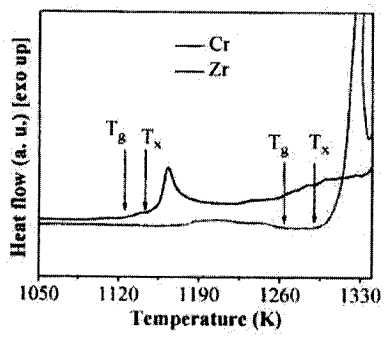

Figure 4. DTA traces for FeBSiM alloys, showing the T_g and T_x: (a) M=Cr and (b) M=Zr.

The DTA results show that the crystallization event for the amorphous phase of Cr-containing alloys occurs at ~1289 K (T_x), with a visible glass transition (T_g) at ~1264 K, as shown in Figure 4a. The Zr-containing alloys show a T_x of 1140 K and a T_g of 1124 K (Fig. 4b). The H_v obtained for both composite bulk alloys are 10.24±0.95 GPa and 9.28±0.17 GPa for the Cr and Zr-containing alloys, respectively. As for the hardness tests, the distance between indentations are ~ 2.5 indenter diameters to avoid interaction between the work-hardened regions of the crystalline zones and the plastic deformation waves of the glassy phase. A summary of physical properties for both composite alloys are shown in Table 1. The magnetic properties are

investigated with VSM and MTGA. The $\mu_0 M_s$ (within experimental uncertainty) is 1.25±0.02 T for the Cr-containing alloy and 0.97±0.01 T for the Zr-containing alloy (Figs. 5a-b) and the MTGA curves (Figs. 6a-b) show two magnetic transitions for both alloys. These transitions can be associated with different magnetic phases.

Table I. Mechanical, thermal and magnetic properties for the investigated FeBSiM alloys.

M	H_v (GPa)	T_g (K)	T_x (K)	ΔT_x (K)	T_c^{am} (K)	$\mu_0 M_s$ (T)
Cr	10.24±0.95	1264±10	1289±10	25±3	410±5	1.25±0.02
Zr	9.28±0.17	1124±10	1140±10	14±3	400±5	0.97±0.01

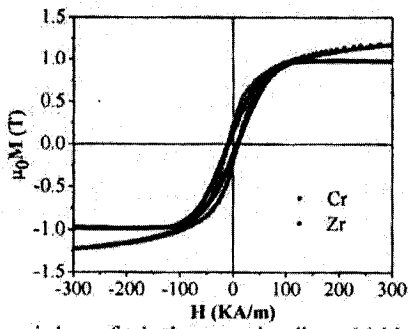

Figure 5. Hysteresis loops for both composite alloys: (a) M=Cr and (b) M=Zr alloys.

For the bulk composite M=Cr alloy (Fig. 6a) two T_c are evident at T_{c1}=410 K and T_{c2}=955 K. The T_{c1} transition can be ascribed to the amorphous phase, since related glassy $Fe_{1-x}B_x$ and Fe-B-Si alloys show a maximum T_c value at ~740 K [9,10]. Based on this, a high temperature regime for T_c values can be defined as T>740 K, in which T_{c2} is contained. These values of high temperatures coincide very well with the T_c of crystalline $Fe_{92}Si_8$ phase (T_c=950 K [9]). Similarly, the bulk composite alloy M=Zr also presents two T_c (shown in Fig. 6b). Again the low temperatures T_{c1}=400 K can be associated to the amorphous phase as is mentioned before, whilst the high temperature T_{c2}=1010 K should be corresponding to Fe_2B phase (with T_c=1015 K [11,12]). Additionally Figure 6c shows a curve obtained from the Cr-containing alloy after heat treatment at 1200 K for 8 hours. It can be seen that the Curie transition corresponding to the amorphous phase disappears after this treatment confirming the existence of this phase in the as-cast alloys. These results agree with the SEM and TEM analysis.

DISCUSSION

The composite nature of the bulk $Fe_{72}B_{19.2}Si_{4.8}M_4$ (M=Cr, Zr) alloys are verified by XRD, SEM, MTGA and TEM results. With these results, it is possible to point out the presence of the crystalline phases Fe_2B and $Fe_{92}Si_8$. It is also found that these phases are dispersed within the amorphous phase, generally having a compositional variance of Fe content. For both composite alloys, the crystallization event of the amorphous phase consists of a single stage. The high T_x observed for the amorphous phase are indeed among the highest T_x reported in, at least, the Fe-based glassy alloy family [13,14]. This enhancement of the resistance to devitrification can be

explained by the addition of Cr/Zr atoms with a large atomic radii (r_{Zr}=0.160 nm and r_{Cr}=0.125 nm [15]), relative to the B atom (with r_B=0.082 nm [15]).

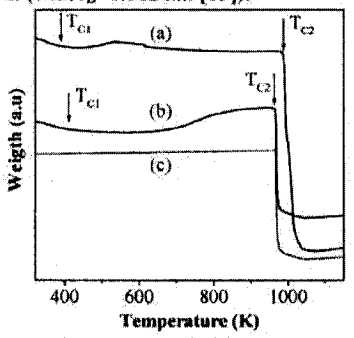

Figure 7. MTGA traces for alloys: (a) as-cast M=Zr, (b) as-cast M=Cr and (c) crystallized M=Cr.

The combined presence of large/small atomic species promotes a more efficient occupancy of interstitial spaces among major constituent atoms, yielding to an improved packing density of the liquid and hence, to the hindering of the crystallization process. Moreover, the high T_x caused by the minor addition of these elements means that the atoms will need more energy to form the critical nuclei, and therefore, a larger critical size would be needed to become a nucleation site. This leads to a higher activation energy for the nucleation and growth processes during crystallization.

The H_v recorded for the M=Zr alloy is found to be higher than some shock-resisting steels (S and M50 type), whose maximum hardness is 7.57 Gpa [16]. For a homogeneous glass structure, it has previously been found that thermal stability, expressed by T_g or T_x, correlates quite well with mechanical properties, such as H_v, at least within a particular alloy system [17]. Nevertheless, the fact that the obtained H_v results are the hardness average of the glassy and crystalline phases restrict comparison but they provide an idea of the bulk hardness of the aforementioned composite alloys. Additionally, the H_v hardness values of both bulk composite alloys can be directly associated with the hardness of the $Fe_{92}Si_8$ and Fe_2B crystalline phases, since this crystalline intermetallic phase is harder and stiffer than the glassy one. The observed $\mu_0 M_s$ results for Cr-containing alloy are comparable with the saturation polarization of the best low-boron, FINEMET-type alloys ($Fe_{73.5}Si_{13.5}B_9Nb_3Cu_1$), in which the maximum $\mu_0 M_s$ value of 1.25 T is reported [18]. These excellent $\mu_0 M_s$ values result from the contribution of the amorphous and crystalline magnetic phases with the latter having $\mu_0 M_s$ as high as 1.68 T ($Fe_{92}Si_8$ [11]) and 1.40 T (Fe_2B [9]). Similarly, the T_c values observed for the amorphous phases (within the temperature range 400 - 450 K, Table I) of the composite alloys investigated compare very well with the T_c of similar FINEMET-type alloys (between 360 and 843 K [19]). These good values of T_c for the current bulk composite alloys might also be attributed to the considerably large atomic radius of Cr and Zr in comparison to the atomic radius of B. It is thought that the inclusion of such big atoms can produce an enhancement of the integral exchange between magnetic atoms, via an enlargement of the nearest Fe-Fe interatomic distances, and hence, the observed high T_c. Additionally, the increasing values for the T_c of the amorphous phase for both

bulk composite alloys can be a consequence of the variable Fe:B ratio observed within the glassy matrix which also affects the first neighbour Fe-Fe separation.

CONCLUSIONS

Bulk composite $Fe_{72}B_{19.2}Si_{4.8}M_4$ (M=Cr, Zr) alloys are successfully produced by copper mould injection casting. The results of T_r are very promising and supersede the range of temperatures at which these alloys are normally exposed. The values of H_v for both alloys are surprisingly higher than some high speed steels. Concerning the magnetic properties, the Cr-containing alloy has a saturation polarization value of 1.25±0.02 T, which is as good as some Fe-Si-B amorphous alloys. The aforementioned properties can be produced by the addition of atoms with a large atomic radii and the constructive interaction between crystalline and amorphous phases.

ACKNOWLEDGEMENTS

The authors are grateful to Adriana Tejeda, Gabriel Lara, Esteban Fregoso-Israel, Omar Novelo, Carlos Florez Morales and Hermilo Zarco for their valuable technical assistance. S. Báez also acknowledges the scholarship granted by CEP, UNAM.

REFERENCES

[1]. Functional Materials, European Conference on Advanced Materials and Processes, Euromat, K. Grassie, E. Tenckhoff, G. Wegner, J. Haubelt and H. Hanselka (Eds), Vol. 13, Wiley-VCH, Weinheim, 2000.
[2]. Materials Science Forum, Y. Umakoshi, S. Fujimoto (Eds), Vol. 512, Trans. Tech. Pub. LTD, Beijing 2006.
[3]. Magnetism, materials and applications, É du Trémolet de Lacheisserie (Ed), Springer, New York, 2005.
[4]. K. H. J. Buschow, Handbook of Magnetic Materials. Vol. 10. K. H. J. Buschow (Ed), Elsevier Science, Holland, 1997.
[5]. B. D. Cullity and C. D. Graham, Introduction to Magnetic Materials, 2nd Ed., IEEE Press Wiley, Hoboken, 2009.
[6]. R. M. Bozorth, Ferromagnetism, Van Nostrand, New York, 1968.
[7]. W. Klement, R. H. Willens and P. Duwez, Nature 187 (1960) 869.
[8]. R.E. Smallman and A.H.W. Ngan, Physical Metallurgy and Advanced Materials, Seven Edition (2007) p.40.
[9]. R. Hasegawa and R. Ray, J. App. Phys. 49 (1978) 4174
[10]. H.S. Chen, Rep. Prog. Phys. 43 (1980) 402.
[11]. M.F. Littmann, IEEE Trans. Magn. 1 (1971) 48.
[12]. L.I. Berger and B.R. Pamplim, Handbook of Chemistry and Physics, CRC, Section 12, Properties of Solids, D.R. Lide (ed) (2005-2006) p.93.
[13] W.H. Wang, C. Dong and C.H. Shek, Mater. Sci. Eng. R 44 (2004) 45.
[14]. Z. Long, H. Wei, Y. Ding, P. Zhang, G. Xie and A. Inoue, J. Alloys Comp. 475 (2009) 207.
[15]. O.N. Senkov and D.B. Miracle, Mater. Res. Bull. 36 (2001) 2183.

[16]. American Society for Metals, Handbook Vol.1, Properties and selection: Irons, Steels and High-Performance Alloys, Wrought Tool Steels, A.M. Bayer, T. Vasco and L.R Walton (Rev.) (1990) p.757.
[17]. I.A. Figueroa, R. Rawal, P. Stewart, P.A. Carroll, H.A. Davies, H. Jones and I. Todd, J. Non-Cryst. Solids 353 (2007), p. 839.
[18]. K. Suzuki, in: Y. Liu, D.J. Sellmyer, D.Shindo (Eds.), Processing and modeling of novel nanocrystalline soft magnetic materials, (Tsinghua University Press-Springer, China, 2006) p.340.
[19]. M.E. McHenry, M.A. Willard and D.E. Laughlin, Prog. Mater. Sci. 44 (1999) 291.